Numerical Simulation of Sleeve Repair Welding of In-Service Gas Pipelines

A model was developed to predict conditions for sucessful sleeve repair of in-service gas pipelines

BY I.-W. BANG, Y.-P. SON, K. H. OH, Y.-P. KIM, AND W.-S. KIM

ABSTRACT. The purpose of this study is to develop an appropriate numerical model for full encirclement, sleeve repair welding of in-service gas pipelines and to investigate the effects of in-service welding conditions. An axisymmetric finite element model was used to calculate the temperature distribution, maximum HAZ hardness, and the distribution of residual stress and plastic strain during multipass sleeve fillet welding of in-service API 5L X65 pipelines of 14.3 mm thickness. Experiments were also conducted for sleeve repair welding on pipe with internal pressure. The calculated geometry of the fusion zone and HAZ was in good agreement with the macrostructures of sleeve repair fillet welds. The calculated maximum HAZ hardness was in good agreement with the measured value. The effect of gas flow rate on the maximum HAZ hardness and the effects of internal pressure on residual stress and plastic strain distribution were investigated. Risk of melt-through and susceptibility to cold cracking were also estimated using a simplified analysis.

Introduction

In buried natural gas pipelines, defects can occur as a result of construction faults, corrosion, third-party interference, and ground movement. When a segment of a pipeline is found to be defective, one of the repair methods is to vent the gas within the pipeline and cut out the defective segment after shutting down the pipeline. However, the cost is extremely high in terms of venting and stopping the gas supply. Therefore, most pipeline companies have developed repair methods without stopping flow through the pipe. These in-service repair methods are widely used throughout the natural gas, petroleum and petrochemical industries (Refs. 1–4). Welding onto a gas pipeline in operation, known as in-service welding, is a frequently employed repair technique. The direct deposition of weld metal, sleeve repair welding, and hot-tap welding are typical examples of in-service welding.

There are two important concerns with welding on in-service pipelines. The first concern is the possibility of melt-through due to localized heating, leading to loss of material strength on the inner surface of pipe during the welding process. The pipe wall can burst under internal pressure if the loss of the strength is large.

The second concern is the high cooling rate of the weld as a result of flowing gas quickly removing heat from the pipe wall. The high cooling rate can promote the formation of heat-affected zone (HAZ) microstructure with high hardness, making these weldments susceptible to cold cracking and sulfide stress cracking in sour service. The rapid cooling can be compensated by increasing heat input, but the increased heat input can promote weld penetration and the possibility of melt-through. Thus, suitable welding procedures must ensure optimal HAZ hardness, no melt-through, and proper heat input.

Over the 12-year period between 1978 and 1990, a series of hot-tap welding research programs was carried out at Battelle and Edison Welding Institute (EWI) (Refs. 5–7). A thermal analysis model, based on the two-dimensional finite difference method, was developed to simulate sleeve and direct-branch in-service welding. The cooling rate of the HAZ and the maximum inside surface temperature were predicted for a given pipe geometry and a set of welding parameters. The HAZ hardness was estimated from the cooling rate at 540°C (1000°F) and the carbon equivalent of the material. Taking Vickers hardness 350 HV as a low cracking potential, the maximum inside surface temperature of 982°C (1800°F) was regarded as the limiting maximum temperature to prevent melt-through for low-hydrogen-electrode welding. However, the estimation of HAZ cracking was highly simplified and not applicable to today's high-strength pipeline steels. Also, melt-through limits were predicted only by the maximum inside surface temperature and the effects of internal pressure and stresses were not considered.

The finite element method offers a computational tool for simulation and analysis of in-service welding of gas pipelines (Refs. 8–10). In addition to investigating the transient thermal field and cooling rates by thermal analysis, stress field and melt-through have been analyzed using a thermoelastic-plastic model or thermoelastic-viscoplastic model by the finite element method. Sabapathy et al. (Ref. 10) predicted melt-through using a thermoelastic-plastic model and also developed an alternative and convenient method to predict the bursting pressure during in-service fillet welding.

Presently, repair welding on an in-service natural gas pipeline is a primary concern of Korea Gas Corporation (KOGAS). Therefore, a systematic study was undertaken for the repair welding of API 5L X65 main pipeline operating under the internal pressure of 6.9 MPa (70 kg_f/cm^2), with a diameter of 762 mm and a thickness of 17.5 or 14.3 mm. Following a previous study of bead-on-plate welding and repair welding by direct deposition of

KEY WORDS

Sleeve Repair Welding
Finite Element Method
Melt-Through
Cold Cracking
Residual Stresses
Maximum HAZ Hardness

I.-W. BANG, Y.-P. SON, and K. H. OH are with the School of Materials Science and Engineering, College of Engineering, Seoul National University, Seoul, Korea. Y.-P. KIM and W.-S. KIM are with R & D Center, Korea Gas Corp., Ansan, Korea.

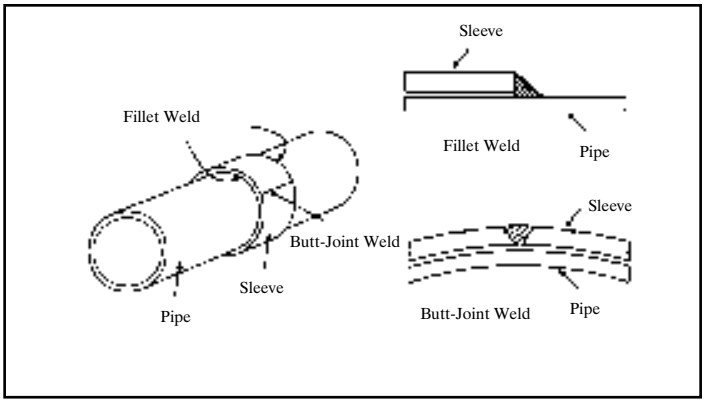

Fig. 1 — Schematic of sleeve repair welding on pipe.

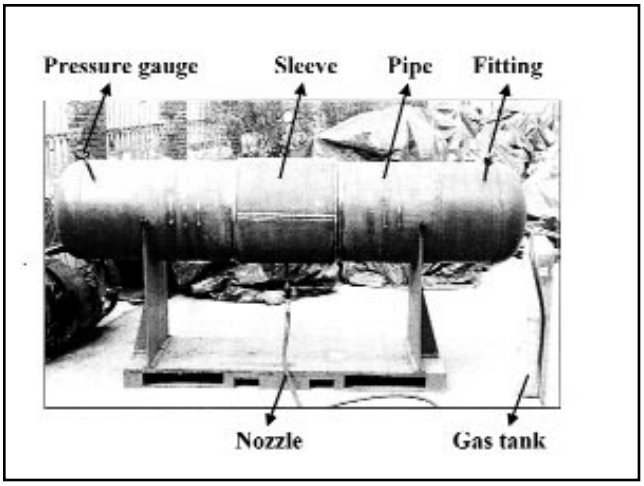

Fig. 2 — Configuration of pressurized sleeve repair welding test equipment at the R and D center of KOGAS Corp.

Table 1 — The Chemical Compositions (wt-%) of the Pipe, Sleeve, and Weld Metal

Elements	C	Mn	P	S	Si	Nb	V	Ti	Ni	Cr	Mo	C_{IIW}[a]
Pipe (sleeve)	0.06	1.69	0.020	0.001	0.25	0.034	0.062	0.022	0.018	0.027	0.001	0.36
Weld metal	0.04	1.41	0.011	0.003	0.59	0.004	0.008	0.021	0.612	0.043	0.276	0.38

(a) $C_{IIW} = C + Mn/6 + (Ni + Cu)/15 + (Cr + Mo + V)/5$.

Table 2 — The Welding Conditions for Sleeve Fillet Welding

Pass Number	Process	Electrode Diameter (mm)	Current (A)	Voltage (V)	Welding Speed (cm/min)	Heat Input (kJ/mm)
1	GTAW	2.4	194	23	16	1.67
2	SMAW	2.6	96	29	5	3.34
3	SMAW	2.6	96	30	9	1.92
4	SMAW	3.2	120	30	5	4.32
5	SMAW	3.2	117	30	10	2.11
6	SMAW	2.6	100	30	7	2.57
7	SMAW	3.2	122	31	5	4.54
8	SMAW	3.2	118	30	9	2.36

Note: An internal pressure of 4.4 MPa was applied with no gas flow condition.

Table 3 — The Welding Conditions for Sleeve Butt-Joint Welding

Pass Number	Process	Electrode Diameter (mm)	Current (A)	Voltage (V)	Welding Speed (cm/min)	Heat Input (kJ/mm)
1	GTAW	2.4	226	25	13	2.61
2	SMAW	3.2	153	36	12	2.75
3	SMAW	3.2	152	35	11	2.90
4	SMAW	3.2	147	34	15	2.00
5	SMAW	3.2	148	34	13	2.01
6	SMAW	3.2	146	34	17	1.75
7	SMAW	3.2	145	35	17	1.79
8	SMAW	3.2	147	34	18	1.67
9	SMAW	3.2	143	33	17	1.67
10	SMAW	3.2	137	32	17	1.55
11	SMAW	3.2	136	32	18	1.45

Note: An internal pressure of 4.4 MPa was applied with no gas flow condition.

weld metal (Ref. 11), a numerical and experimental study was conducted on in-service sleeve repair welding. The objective of this work was to develop an appropriate numerical model for sleeve repair welding of in-service gas pipelines and to investigate the effects of in-service welding conditions.

An axisymmetric finite element model was developed to simulate multipass sleeve fillet welding on in-service API 5L X65 pipelines of 14.3 mm thickness. The model was used to predict the temperature distribution, maximum HAZ hardness, and the distribution of residual stress and plastic strain. The experimental study was also conducted on sleeve repair welding with internal pressure applied. The calculated maximum HAZ hardness was used to predict the occurrence of cold cracking, and the effect of gas flow rate on the maximum HAZ hardness was investigated. A detailed evolution of residual stress and plastic strain and the effects of internal pressure on their distribution were investigated. An analysis of single-pass fillet welding was also carried out to assess the allowable heat input for sleeve fillet welding.

Experimental Procedure

Full encirclement, sleeve repair welding on in-service gas pipelines is a repair welding method for relatively large de-

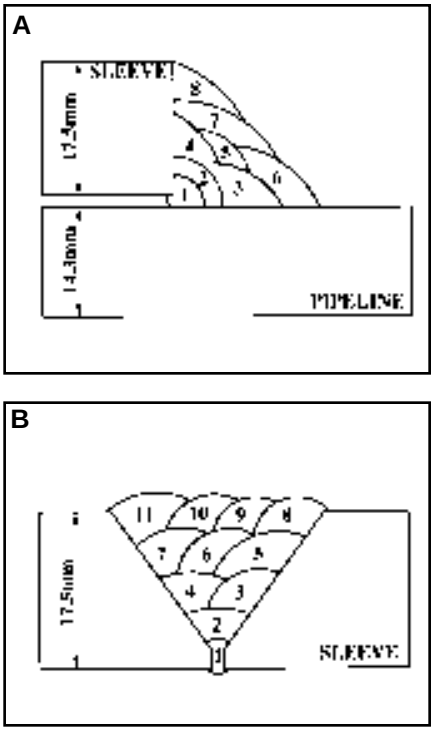

Fig. 3 — Joint shape and pass sequence of sleeve repair welds. A — Fillet welds; B — butt-joint welds.

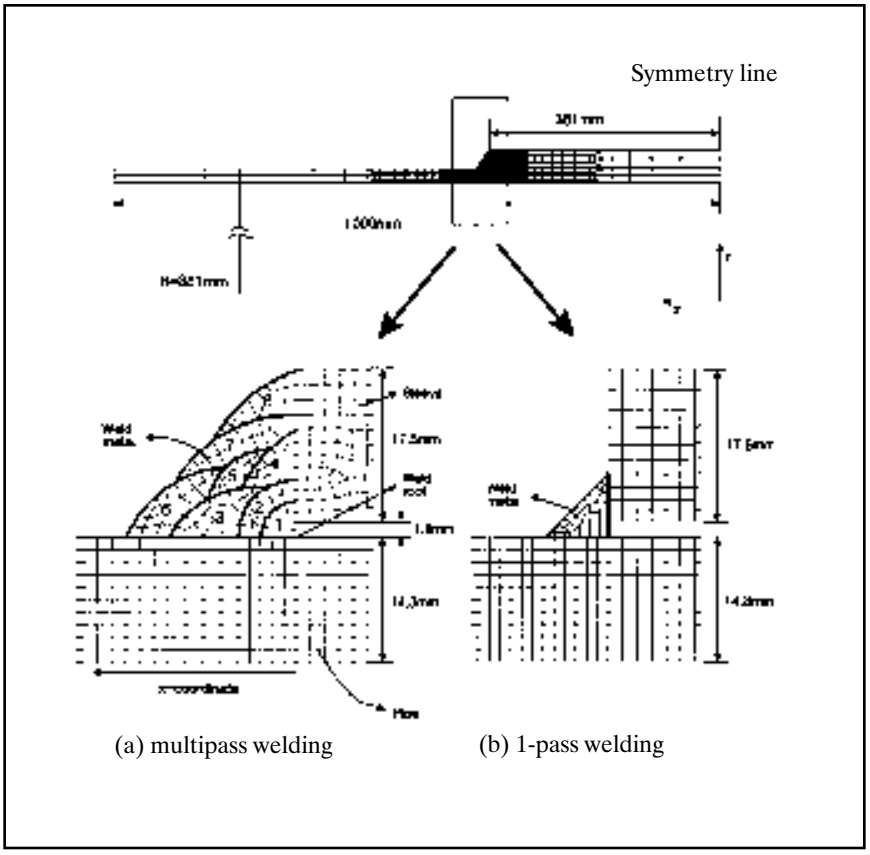

Fig. 4 — Axisymmetric finite element mesh for sleeve fillet welding.

fects. The schematic illustration of this sleeve repair welding method is shown in Fig. 1. Two sleeves are attached to the pipe around damaged sections and then circumferential fillet welding and longitudinal butt-joint welding are performed.

Figure 2 shows the configuration of the pressurized sleeve repair welding test equipment. Both ends of the pipe were welded using the cap made of WPHY 65, and a pressure gauge and a fitting for measuring the gas temperature were installed. In order to simulate the in-service condition, an internal pressure of 4.4 MPa was applied using a nitrogen gas.

The diameter and the thickness of the pipe are 762 and 14.3 mm, and the repair sleeves were made by expanding radially a 762-mm-diameter pipe with a 17.5-mm thickness. The chemical compositions of the API 5L X65 pipe, sleeve, and weld metal are listed in Table 1.

Figures 3A and B show the weld joint shape and welding sequence of sleeve fillet welds and groove welds, respectively. Manual shielded metal arc welding (SMAW) and gas tungsten arc welding (GTAW) processes were applied to sleeve repair welds. The welding conditions for fillet welding and butt-joint welding are shown in Tables 2 and 3, respectively.

In the butt-joint welds, melt-through is a matter of little concern because the weld metal is not in direct contact with the pipe. In this study, fillet welds are in direct contact with a pipe with an internal pressure of 4.4 MPa, but melt-through can be avoided by controlling heat input. Small-diameter electrodes are recommended for welds in contact with the pipe because heat input can be reduced with them (Ref. 12). Small-diameter electrodes were used in this experiment. A 2.4-mm, ER70S-G electrode was used for pass 1, and a 2.6-mm low-hydrogen E9016-G electrode was used for passes 2, 3, and 6. A 3.2-mm low-hydrogen E9016-G electrode was used for the layers that were not in direct contact with the pressure-containing pipe. Preheating was not applied considering the field welding conditions.

The weld joints were sectioned and polished to observe the geometry of the weld metal and the HAZ. The penetration of weld metal and depth of HAZ were measured. Microhardness measurements with a 500-g load were made in base metal, coarse-grained HAZ (CGHAZ), fine-grained HAZ (FGHAZ), and weld metal of pipe and sleeve.

Computational Procedure

The commercial finite element code *ABAQUS* (Ref. 13) was used for the thermal and mechanical analysis. A sequentially coupled analysis of thermal and mechanical analyses was performed. An axisymmetric model was used to calculate the distributions of temperature, residual stresses, and plastic strain during the multipass sleeve fillet welding of in-service API 5L X65 pipeline. The welding conditions listed in Table 2 were used. An analysis of a single-pass fillet weld applied with SMAW was also carried out to assess the allowable heat input.

Finite Element Mesh

The thermal and mechanical response of a weldment is a three-dimensional problem that requires a considerable amount of computational time. The computational time required to simulate multipass welding increases in proportion to the number of weld passes. Therefore, it is necessary to develop cost-effective procedures to reduce computational time while preserving the accuracy of the solution. An assumption common for most analysis of circumferential multipass welding is the assumption of axisymmetry, that is, welding heat is assumed to be deposited at the same time around the circumference. This assumption, which strongly reduces the

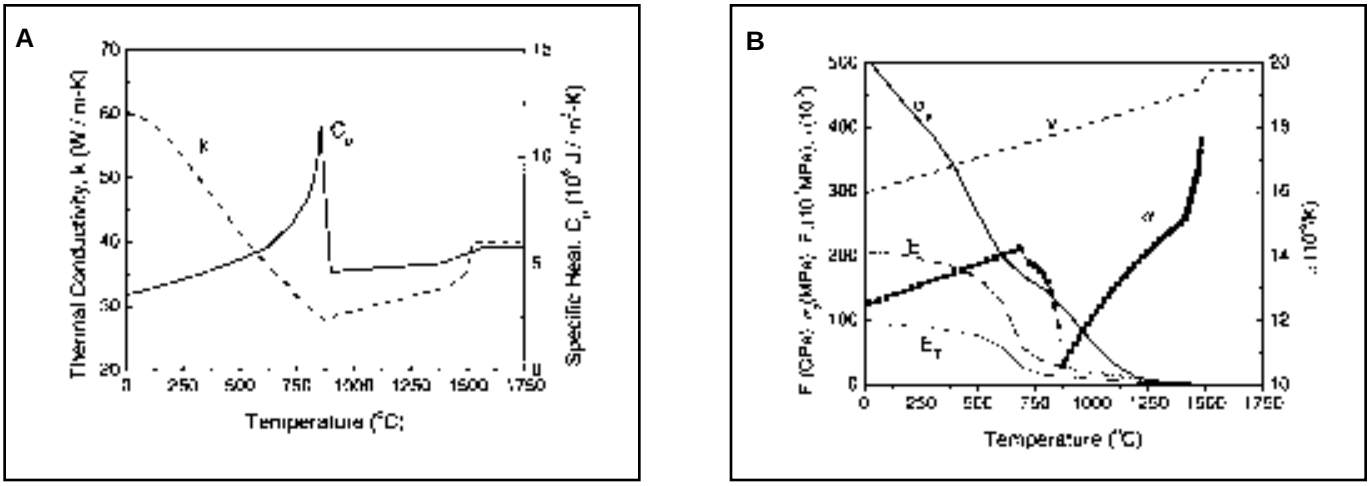

Fig. 5 — Temperature-dependent material properties of API X65 pipe. A — Thermal properties; B — mechanical properties.

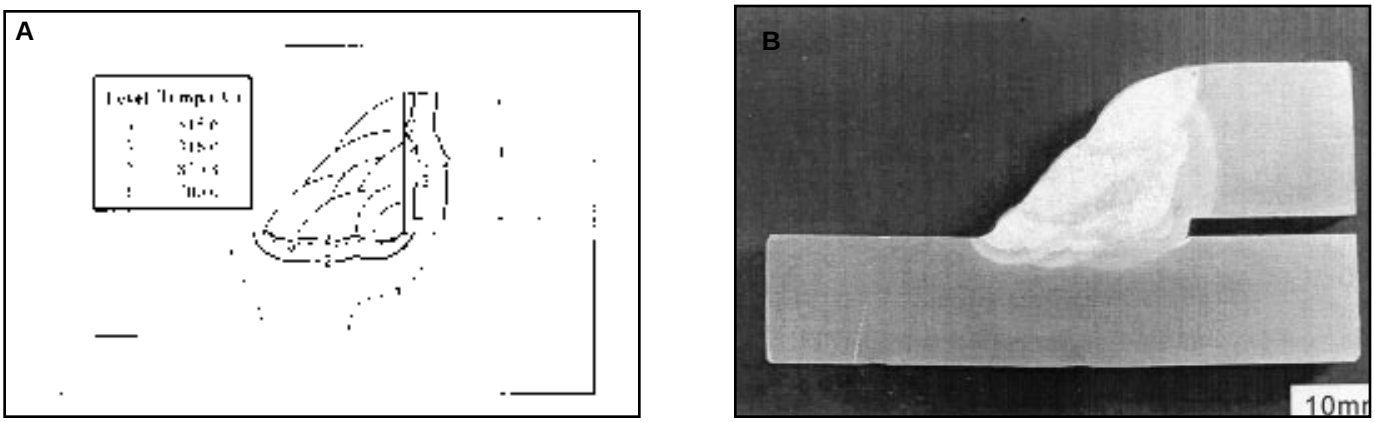

Fig. 6 — Comparison of (A) calculated peak temperature distributions and (B) experimental macrostructures at the welding conditions listed in Table 2.

size of the FE model and the CPU time needed, can be justified by observation in experiments that residual stresses in circumferential groove welds are reasonably axisymmetric (Refs. 14, 15). So, a two-dimensional axisymmetric model was used in this study.

Based on the geometry and weld pass sequence shown in Figs. 2 and 3, an axisymmetric finite element mesh for sleeve fillet welding was made as shown in Fig. 4. In Fig. 4, the r-coordinate and z-coordinate correspond to the radial and axial direction of the pipe, respectively, and the welding direction is hoop direction. The x-coordinate was defined along the inner surface of pipe in order to describe the distributions of residual stresses and strain. The origin of the axis corresponds to the position at the inner surface of the pipe below the weld root.

Actual circumferential sleeve fillet welding is performed sequentially or simultaneously at both left and right sides of a sleeve. Assuming the welding is performed simultaneously at both left and right sides of a sleeve, half of the geometry was modeled by applying the symmetry condition at the centerline of the axial direction. The finite element model of Fig. 4A consists of 750 quadrilateral elements and 919 nodes. A refined finite element mesh was used in and near the weld region.

Modeling of one-pass welding is an efficient way to investigate the effects of heat input on penetration, melt-through, and cold cracking. The finite element mesh for single-pass welding near the weld region is shown in Fig. 4B. The geometry of the pipe and sleeve is equal to that of the finite element mesh of Fig. 4A and only the mesh of weld metal was changed in the simple triangular geometry.

The area of weld metal (weld bead reinforcement) was assumed to be proportional to heat input. The SMAW process was used for modeling single-pass welding.

Thermal Analysis

To simulate arc heating effects efficiently during multipass welding, the equivalent heat input can be assumed as the combination of both surface and body heat flux components (Ref. 14). The total heat input can be given as follows:

$$Q = Q_s + Q_b = \eta E I \qquad (1)$$

where Q_S and Q_B are the heat input due to surface flux and body flux, respectively, η is the arc efficiency, E is voltage, and I is current. The ratio of Q_B/Q_S can be adjusted to achieve an accurate representation of the fusion zone. In this study, the total heat input was assumed to be 20% of surface flux and 80% of body flux from the comparison between the experimental and the calculated size of the fusion zone. The arc efficiencies used in the analysis are 0.75 for SMAW and 0.40 for GTAW.

The surface flux q_S and body flux q_B are

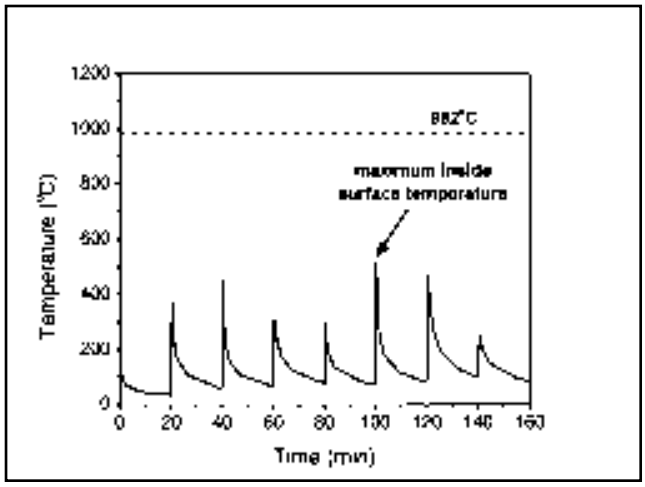

Fig. 7 — Variation of temperature with time at the position where the peak temperature is maximum on the inner surface of the pipe at the welding conditions listed in Table 2.

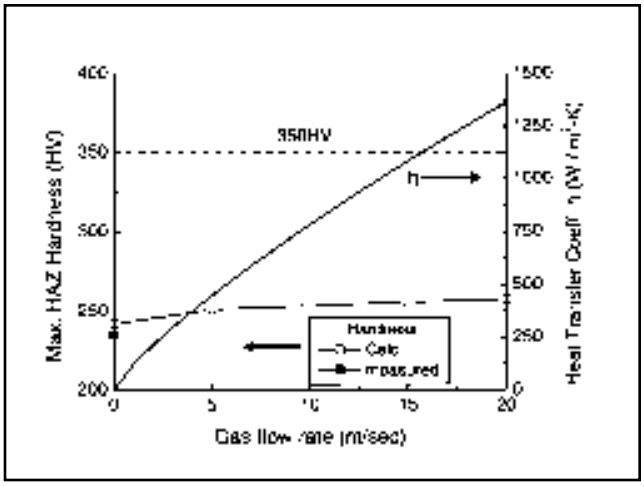

Fig. 8 — Effect of gas flow rate on maximum HAZ hardness for the welding conditions in Table 2 with the exception of the gas flow condition.

generally represented in the form of a Gaussian distribution as follows (Ref. 16):

$$q_s = \frac{3Q_s}{\pi ac} exp\left(-\frac{3x^2}{a^2} - \frac{3z^2}{c^2}\right) \quad (2)$$

$$q_B = \frac{6\sqrt{3}Q_B}{abc\pi\sqrt{\pi}} exp\left(-\frac{3x^2}{a^2} - \frac{3y^2}{b^2} - \frac{3z^2}{c^2}\right) \quad (3)$$

where *a, b,* and *c* are the semicharacteristic arc dimensions in *x, y,* and *z* direction. This heat source model has often been used to approximate simple welding processes carried out in the flat position, i.e., welding horizontally in a straight line on a horizontal flat plate with the electrode perpendicular to the plate (Ref. 10). A characteristic of a low-hydrogen electrode is often a shallow penetration, which suggests a heat distribution flatter and more evenly distributed than Gaussian. Sabapathy et al. (Ref. 10) modified the Gaussian heat source model by changing the exponential terms and simulated in-service welding. In this study, the heat fluxes of Equations 2 and 3 were modified by assuming the uniform distribution of heat fluxes in width and thickness direction in order to simulate the shallow penetration. The surface and body fluxes can be given as follows:

$$q_s = \frac{\sqrt{3}Q_s}{ac\sqrt{\pi}} exp\left(-\frac{3z^2}{c^2}\right) \quad (4)$$

$$q_B = \frac{\sqrt{3}Q_B}{Ac\sqrt{\pi}} exp\left(-\frac{3z^2}{c^2}\right) \quad (5)$$

where A is the cross-sectional area of the fusion zone. The values of a and c were chosen as the half width of the fusion zone. The fixed z-coordinate is related to the moving coordinate as follows:

$$z = v(\tau - t) \quad (6)$$

where v is the welding speed and τ is a lag factor to define the position of the heat source at time $t = 0$.

The element birth technique was used to model the multipass weld metal deposition effects (Ref. 13). The elements of each weld pass were meshed separately and then connected to adjacent passes and the base metal mesh with contact surfaces. The weld metal finite elements and contact surfaces were inactive at the beginning of the analysis, and then activated at the specified time to simulate the deposi-

Table 4 — Thermophysical Data of Natural Gas (Ref. 7)

Property	Value
Specific heat of gas, C_{pg}	2245.36 J/kg-K
Density of gas, ρ_g	36.9 kg/m^3
Thermal Conductivity of gas k_g	3.5354 X 10^{-2} w/m-K
Viscosity of gas, μ_g	1.11 X 10^{-5} Pa-s

Table 5 — Vickers Hardness of Sleeve Fillet Welds

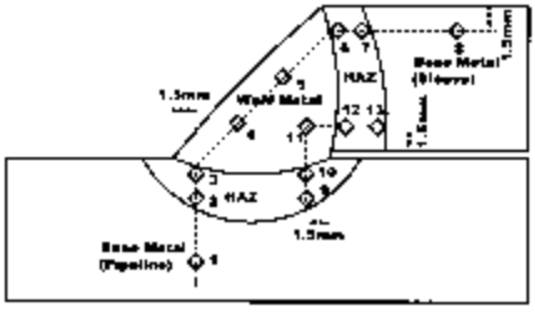

Location		Hardness (HV)
Weld metal	SMAW (4, 5)	219.0
	GTAW (11)	211.0
CGHAZ	Pipe (3, 10)	235.0
	Sleeve (6, 12)	213.0
FGHAZ	Pipe (2, 9)	202.5
	sleeve (7, 13)	196.5
Base metal	Pipe (1)	178.0
	Sleeve (8)	179.0

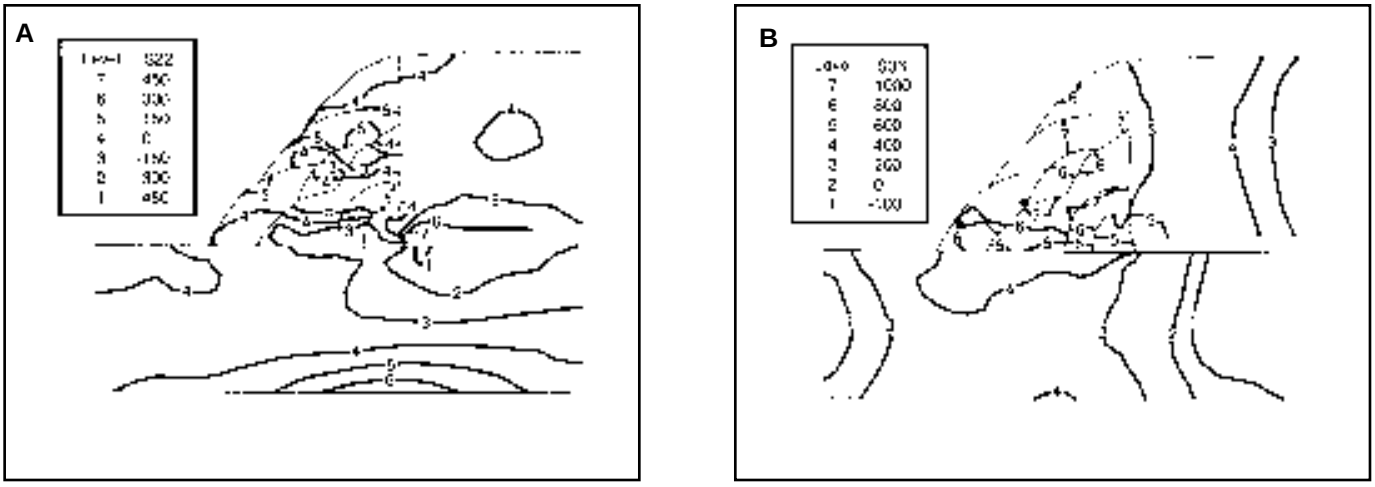

Fig. 9 — Contour plots of residual stress distributions. A — Axial stress; B — hoop stress using the welding conditions listed in Table 2.

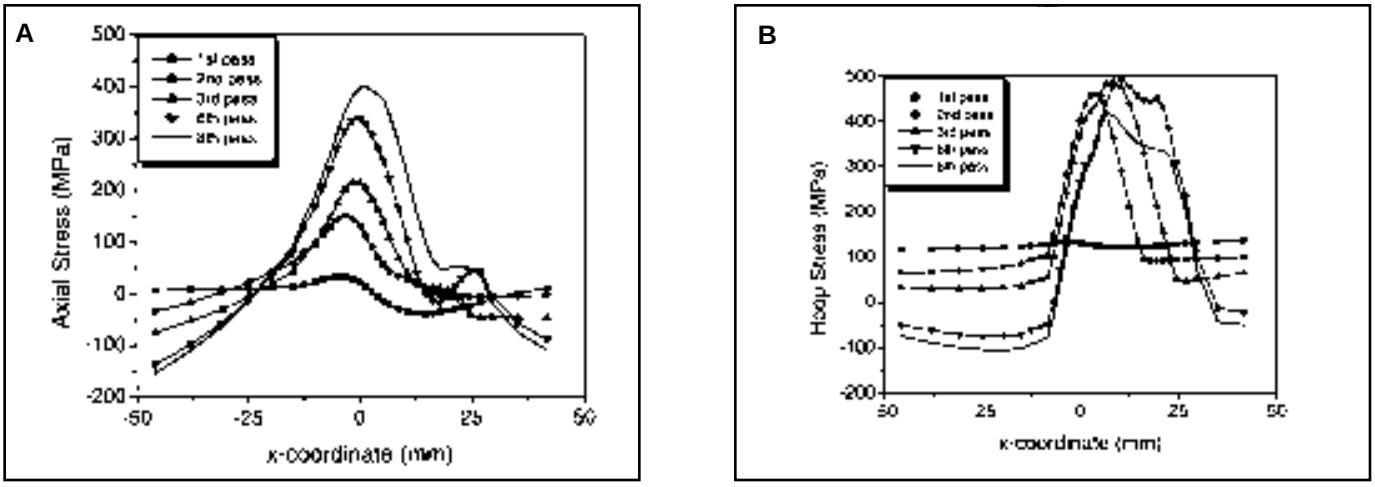

Fig. 10 — Evolution of residual stress along the inner surface of the pipe. A — Axial stress; B — hoop stress using the welding conditions listed in Table 2.

tion sequence of weld passes.

The temperature-dependent thermal conductivity and specific heat of pipe material were obtained from the chemical composition of the pipe material, as shown in Fig. 5A (Ref. 17). The latent heat of fusion 2.1 x 10^9 J/m^3 was used to model the solid-liquid transformation.

The inner and outer surfaces of the pipe and sleeve are subjected to a combination of natural convection, forced convection, and radiation at high temperature. The natural convection and radiation boundary condition were used at the outside of the sleeve and the outer surface of the pipe. The heat transfer mechanism at the inner surface of the pipe was taken as a natural convection, a radiation boundary condition at the condition of no gas flow, and as a forced convection boundary at the condition of gas flow. The convective heat transfer between pipe and flowing gas was characterized with a heat transfer coefficient, h_g, determined from the following dimensionless relation (Ref. 18):

$$\frac{h_g D}{k_g} = 0.023\left(\frac{\rho_g \nu_g D}{\mu_g}\right)^{0.8}\left(\frac{C_{pg}\mu_g}{k_g}\right)^{0.4} \quad (7)$$

where D is the pipe diameter, ν_g is the velocity of the gas, μ_g is the viscosity of the gas, and h_g is the heat transfer coefficient between pipe and flowing gas. Thermophysical data to calculate h_g are listed in Table 4 (Ref. 7).

Mechanical Analysis

Temperature histories from the thermal analysis were given as inputs for the mechanical analysis. Similar to the thermal model, the filler metal passes were tied to adjacent passes and the base metal with contact surfaces. It is also possible to use the element birth technique in the mechanical analysis. However, this may give serious numerical problems in the mechanical analysis because inactive elements at the boundary between old, already deposited material, and new material deposited in the particular weld pass may be strongly distorted when being activated. Attempts to fit the undeformed filler material to the deformed geometry will lead to a stress buildup in this stress-free material and a redistribution of residual stresses from previous passes. Moreover, the computation will break down immediately if the magnitudes of deformation of the inactive elements exceed the size of the elements.

Troive and Johnson (Ref. 19) modified the common element birth technique where the degrees of freedom for all unique birth nodes are fully constrained until the time of birth by changing the con-

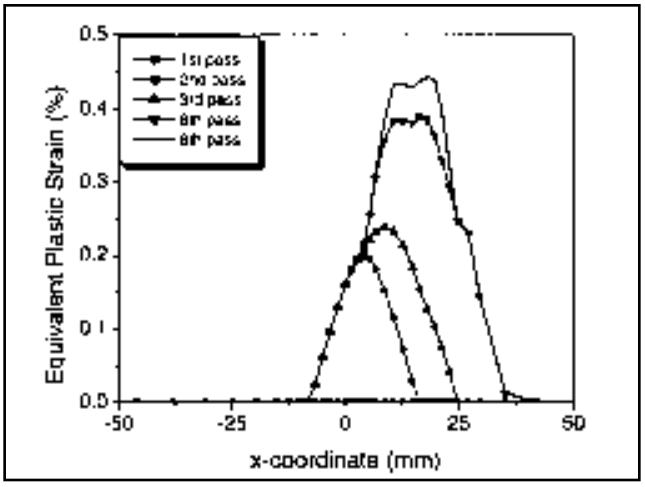

Fig. 11 — Evolution of equivalent plastic strain along the inner surface of the pipe using the welding conditions listed in Table 2.

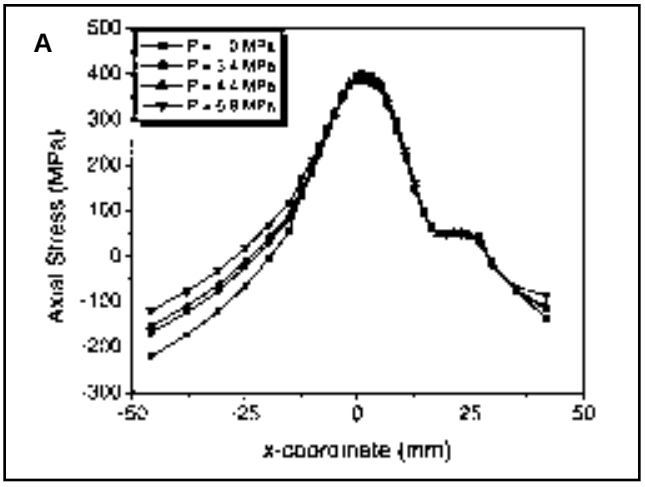

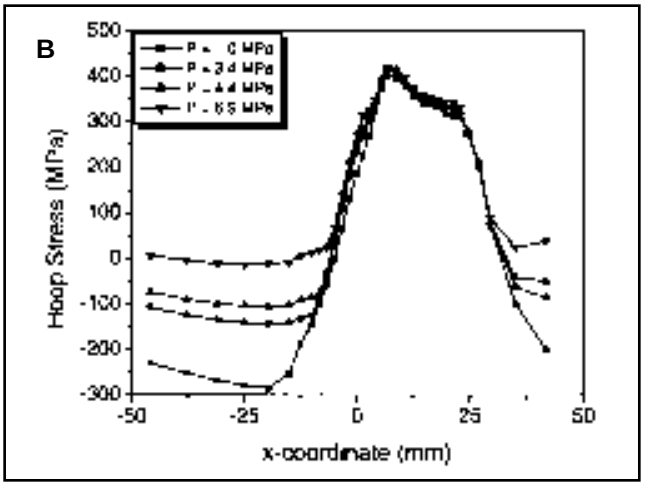

Fig. 12 — Effect of internal pressure on residual stress distribution along the inner surface of the pipe. A — Axial stress; B — hoop stress using the welding conditions listed in Table 2.

ditions for all birth nodes to be totally free, even if not activated. By this technique, the deformation field of the distorted unactivated elements will be smoothed out over the area of unactivated elements, and thereby high magnitudes of element distortions will be avoided. Another approach is to keep the unactivated elements at a high temperature. These elements will then have a low stiffness and not affect any deformation mechanism even though they were present. The latter method was used in the present study.

The thermoelastic-plastic constitutive model was used to describe the deformation behavior. Figure 5B shows the temperature-dependent mechanical properties, i.e., Young's modulus E, yield stress σ_y, hardening modulus E_T, poisson's ratio ν, and thermal expansion coefficient α. The true yield stress of pipe material at room temperature is 503 MPa. The thermal expansion coefficient was set to be zero above melting temperature to prevent stress being applied to the liquid.

The pressure loading by internal pressure was applied at the first step of the mechanical analysis, and then the thermal loading from the temperature histories was applied, preserving the pressure loading.

Assessment of Cold Cracking

Cold cracking, or hydrogen-induced cracking, is one of the most serious problems encountered during welding. Depending on the location of the cold crack, it is called underbead crack, root crack, or toe crack. Major factors that contribute to cold cracking are susceptible microstructure of high hardness, hydrogen content, and tensile restraint stresses.

These factors mutually interact, and it is difficult to simply evaluate the effect they may have on cold cracking susceptibility. Generally, the maximum HAZ hardness is regarded as an approximate index for susceptibility to cold cracking. The maximum HAZ hardness is often limited to 350 HV in welding fabrication of offshore structures and line-pipes for avoidance of cold cracking (Refs. 20, 21). A previous study showed HAZ microstructures with hardness of 248 HV and higher are susceptible to stress corrosion cracking (SCC) when the welding is done on in-service pipelines used to transport mildly sour gas (Ref. 22).

The formulas for estimating maximum HAZ hardness can be separated into three different groups (Ref. 23): 1) formulas that estimate hardness entirely from carbon equivalents; 2) formulas that estimate hardness from various carbon equivalents in conjunction with welding parameters, such as cooling time $t_{8/5}$; and 3) formulas that estimate hardness by means of various carbon equivalents in conjunction with microstructure. For the first group, the application of the formulas must be restricted to the circumstances for which they were developed. The formulas belonging to the last group are not as versatile as the formulas from groups 1 and 2 because detailed information on the martensite content, which only can be obtained by detailed metallographic examination, is required in addition to chemical composition. The formula proposed by Kasuya et al. has the widest applicable range among the formulas belonging to group 2 and was reported to show good correlation between measured and estimated maximum HAZ hardness (Ref. 24).

The maximum HAZ hardness in the formula proposed by Kasuya et al. is given as follows:

$$HV = (H_M + H_B)/2 - (H_M - H_B) \cdot \arctan(X)/2.2 \quad (8)$$

where H_M is the hardness value where martensite volume fraction reaches 100% in CGHAZ and H_B is where martensite volume fraction becomes almost 0% in CGHAZ. X is defined by the following equation:

$$X = 4 \cdot \log(\tau/\tau_M)/\log(\tau_B/\tau_M) - 2.0 \quad (9)$$

where τ is the cooling time between 800 and 500°C ($t_{8/5}$), and τ_M and τ_B are the cooling times corresponding to H_M and H_B, respectively. The four constants (H_M, τ_M, H_B and τ_B) depend on the chemical composition of steel (wt-%) and are defined from the experimental data of vari-

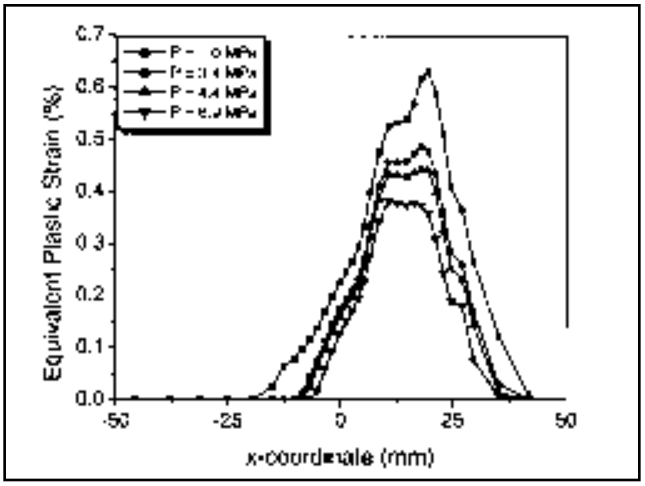

Fig. 13 — Effect of internal pressure on equivalent plastic strain distribution along the inner surface of the pipe using the welding conditions listed in Table 2.

ous steels as follows:

$$H_M = 884C(1–0.3C^2) + 297 \quad (10)$$

$$\tau_M = exp(10.6CE1 – 4.8) \quad (11)$$

where $CE1 = Cp + Si/24 + Mn/6 + Cu/15 + Ni/12 + Cr(1 – 0.16\sqrt{Cr})/8 + Mo/4 + \Delta H$; $Cp = C(C \leq 0.3), C/6 + 0.25 (C > 0.3)$; $\Delta H = 0(B \leq 1$ ppm), $0.03f_N(B = 2$ ppm), $0.06f_N(B = 3$ ppm), $0.09f_N(B \geq 4$ ppm); and $f_N = (0.02 – N)/0.02$

$$H_B = 145 + 130 \tanh(2.65CE2 – 0.69) \quad (12)$$

where $CE2 = C + Si/24 + Mn/5 + Cu/10 + Ni/18 + Cr/5 + Mo/2.5 + V/5 + Nb/3$

$$\tau_B = exp(6.2CE3 + 0.74) \quad (13)$$

where $CE3 = Cp + Mn/3.6 + Cu/20 + Ni/9 + Cr/5 + Mo/4$.

Equations 8–13 were used to predict maximum HAZ hardness from the chemical composition and calculate cooling time from thermal analysis in this study. The occurrence of cold cracking was assessed by the comparison between the calculated maximum HAZ hardness and the limiting hardness of 350 HV. This approach to predict maximum HAZ hardness and the occurrence of cold cracking was successfully applied in the analysis of bead-on-plate welding of API 5L X65 plates with the various welding conditions (Ref. 25).

Results and Discussion

Temperature Distributions

The geometry of the fusion zone and HAZ can be predicted from the peak temperature distributions. The peak temperature distributions were obtained from the calculated transient temperature field. The fusion zone is determined by the melting temperature and the geometry of the HAZ can also be determined by Ae_3 temperature. The HAZ consists of several subzones, which are normally defined by the peak temperatures. Lundin et al. (Ref. 26) reported the average peak temperatures of 1316°C and 954°C are commonly used to represent CGHAZ and FGHAZ, respectively.

Figure 6A shows the calculated peak temperature distributions for the weld zone. The isothermal lines of 1515.6°C, 1316.0°C, and 870.8°C correspond to melting, CGHAZ, and Ae_3 temperatures, respectively. Figure 6B shows the macrostructures of fillet welds. It can be seen that the size and shape of the fusion zone and HAZ observed in macrostructures are in good agreement with the isothermal lines of melting temperature and Ae_3 temperatures, respectively. From the agreement between calculated and experimental weld geometries, it is known the temperature distributions for multipass sleeve fillet welding can be satisfactorily calculated from the model.

Figure 7 shows the variation of temperature with time at the position where the peak temperature is maximum on the inner surface of the pipe. The temperature profile has higher values when the welds are in contact with the pipe, such as passes 2, 3, and 6, rather than when in contact with the sleeve. The highest peak temperature that corresponds to the maximum inside surface temperature was 515°C at pass 6.

This value is much lower than 982°C, which is the limiting maximum inside surface temperature for preventing melt-through (Ref. 7). As shown in Fig. 6B, excessive deformations or melt-through around welds were not observed in welding the pipe with an internal pressure of 4.4 MPa. The heat input of welding pass 4 was 4.32 kJ/mm due to low welding speed, but melt-through was not found numerically nor experimentally.

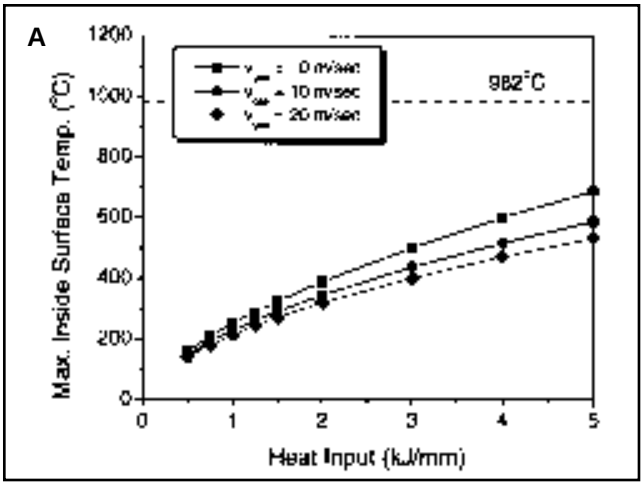

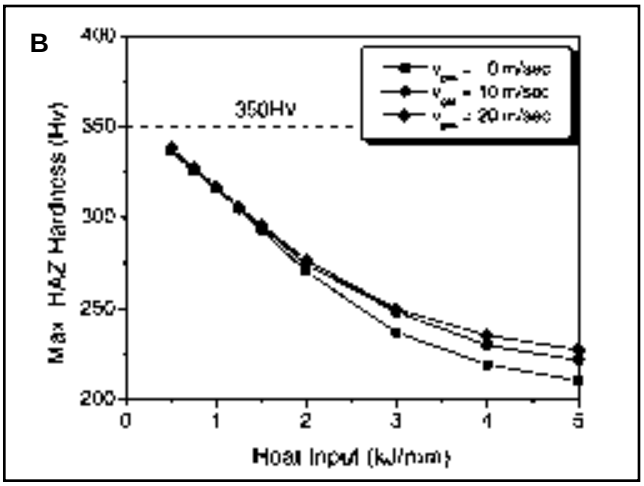

Fig. 14 — Variation of (A) maximum inside surface temperature and (B) maximum HAZ hardness with heat input and gas flow rate for a single-pass sleeve fillet weld.

Hardness Distributions and Effect of Gas Flow Rate on Maximum HAZ Hardness

The measured hardness values for base metal, CGHAZ, FGHAZ, and weld metal are shown in Table 5. The hardness in the CGHAZ of the pipe has the highest value,

235 HV, which is much lower than 350 HV. The calculated maximum HAZ hardness is 242 HV and in good agreement with the measured value. Cold cracks were not observed in the macrostructures of fillet welds, as shown in Fig. 6B.

Natural gas flowing within a pipeline can increase the cooling rate of in-service welds. From the pipeline design standard of Korea Gas Corp., the safe flow rate of natural gas within a pipeline is generally below 18 m/s, and the normal operating flow rate is around 10 m/s. The effect of gas flow rate on the maximum HAZ hardness was numerically investigated at the gas flow rate from 0 to 20 m/s.

As the gas flow rate increases, the heat transfer coefficient of the inner surface of the pipe increases, but the maximum HAZ hardness increases only a little, as shown in Fig. 8. The maximum HAZ hardness at the gas flow rate of 20 m/s is 257 HV, which is only 6% higher than that with no gas flow. This result is in agreement with the fact that cooling rates for thicknesses greater than 0.5 in. (12.7 mm) are little influenced by the fluid inside the pipe (Ref. 7). From Fig. 8, it can be suggested that sleeve repair welding of API 5L X65 pipelines of 14.3-mm thickness with flowing gas can be performed without cold cracking occuring for the given welding conditions.

Residual Stresses and Plastic Strain Distributions

Residual stress and plastic strain are produced by localized heating and cooling during welding. The distributions of residual axial and hoop stresses are shown in Fig. 9. The axial residual stresses at the inner and outer surfaces of the pipe below the weld metal are tensile and compressive, respectively. During heating, the welds are expanded, and the pipe is deformed toward the outside of the pipe. During cooling, the pipe is bent toward the inside by the faster cooling weld region. Therefore, tensile axial residual stress is developed at the inner surface and compressive stress at the outer surface. Hoop stress is tensile at both inner and outer surfaces of the pipe near welds.

Figures 10A and B show the evolution of residual axial and residual hoop stresses along the inner surface of the pipe during welding, respectively. The intermediate residual stress distributions of the weld pass in contact with the pipe and the final residual stress distributions are shown in Fig. 10.

The axial stress at the inner surface gradually increases with each pass sequence as shown in Fig. 10A. The final residual axial stress is tensile within the zone ranging from +30 mm to –20 mm and becomes compressive outside the zone. The maximum value of tensile residual axial stress is found near the origin of the x-coordinate, that is, below the weld root. The hoop stress distributions on the inner surface also show the tendency of gradually increasing with pass sequence as shown in Fig. 10B. The tensile residual hoop stress shows a little decrease at the last pass (pass 8). High tensile hoop stress near the yield stress at room temperature is developed at passes 3 and 6, which are welds in contact with the pipe.

The evolution of equivalent plastic strain along the inner surface is shown in Fig. 11. The plastic strain gradually increases from the second pass to the last pass. The equivalent plastic strain is developed within the zone ranging from +40 mm to –10 mm. The maximum plastic strain is 0.44% at the given welding conditions. The equivalent plastic strain, which characterizes permanent deformation, may be used as an indicator of cumulative damage of the material during the welding process. Because the pipe material has more than 30% elongation, which is much higher than the maximum plastic strain, at a temperature range from room temperature to near 1000°C, it is known the severe loss of material strength or excessive deformation on the inner surface of the pipe will not occur by the above plastic strain. From the calculated plastic strain and the maximum inside surface temperature, it can be suggested the sleeve repair welding of API 5L X65 pipelines of 14.3-mm thickness can be performed without melt-through at the given welding conditions.

Effect of Internal Pressure on Residual Stresses and Plastic Strain

The effect of internal pressure on the residual stresses and plastic strain was investigated varying the magnitude of internal pressure from 0 MPa to the maximum operating pressure of 6.9 MPa. As shown in Fig. 12, the distributions of tensile residual axial and hoop stresses on the inner surface are hardly influenced by the variation of internal pressure. The effect of the increase of hoop stress by internal pressure, which is called Barlow stress, is observed only in the compressive region.

The residual plastic strain decreases as internal pressure increases, as shown in Fig. 13. This is because the bending deformation toward the inside of the pipe during cooling is reduced by internal pressure. In fact, the condition in which internal pressure has a significant effect on in-service welding is that the temperature of the inner surface of the pipe is high enough to cause melt-through.

The calculated maximum inside surface temperature is much lower than the temperature of melt-through generation. From Fig. 13, it can be suggested the sleeve repair welding of API 5L X65 pipelines of 14.3-mm thickness can be carried out without melt-through at the maximum operating pressure of 6.9 MPa.

Allowable Heat Input for Single-Pass Sleeve Fillet Welding

An analysis of single-pass fillet welding was carried out to assess the allowable heat input for sleeve fillet welding. The SMAW process was used and the heat input was varied from 0.5 to 5 kJ/mm. The gas flow rate was varied from 0 to 20 m/s to investigate the effect of gas flow rate on the maximum HAZ hardness.

Figure 14 shows the variations of maximum inside surface temperature and maximum HAZ hardness with the variations of heat input and gas flow rate. The calculated maximum inside surface temperatures show lower values than the melt-through prediction temperature of 982°C for all conditions, as shown in Fig. 14A. The calculated maximum HAZ hardness shows lower values than the limiting hardness of 350 HV for all conditions, as shown in Fig. 14B. From Fig. 14, it is shown melt-through and cold cracking will not occur for a range of heat inputs and gas flow rates for single-pass sleeve fillet welding.

Conclusions

An axisymmetric finite element model was developed to simulate multipass sleeve fillet welding of in-service API 5L X65 pipelines of 14.3-mm thickness. The model was used to predict the temperature distribution, maximum HAZ hardness, and distributions of residual stresses and plastic strain. The calculated geometry of the fusion zone and HAZ was in good agreement with the macrostructures of the sleeve repair fillet welds. The predicted maximum inside surface temperature was much lower than the limiting maximum temperature for preventing melt-through. The calculated maximum HAZ hardness was in good agreement with the measured value and much lower than the maximum allowable HAZ hardness for avoiding cold cracking. Cold cracking was not found in either the numerical simulation or the experiment.

Tensile axial residual stress is developed at the inner surface and compressive stress at the outer surface. The hoop stress is tensile at both inner and outer surfaces of the pipe near welds.

Melt-through was not predicted from the calculated plastic strain distribution and the maximum inside surface temperature. This was confirmed experimentally

by applying internal pressure. The effect of internal pressure on the residual stresses and plastic strain was small. The equivalent plastic strain showed little decrease as internal pressure increased.

From the numerical simulation, it can be suggested the sleeve repair welding of API 5L X65 pipelines of 14.3-mm thickness can be carried out without melt-through at the maximum operating pressure. Melt-through and cold cracking were not predicted for a range of heat input and gas flow rates for single-pass sleeve fillet welding.

References

1. Phelps, B., Cassie, B. A., and Evans, N. H. 1976. Welding onto live natural gas pipeline. *Metal Construction* 8(8): 350–354.

2. Hicks, D. J. 1983. Guidelines for welding on pressurized pipe. *Pipeline & Gas Journal* 210(3): 17–19.

3. Bruce, W. A., and Threadgill, P. L. 1991. Welding onto in-service pipelines. *Welding Design & Fabrication* 64(2): 19–24.

4. Kiefner, J. F. 1994. *Pipeline Repair Manual.* American Gas Association.

5. Kiefner, J. F., and Fischer, R. D. 1988. Models aid pipeline repair welding procedures. *Oil & Gas Journal* 86(10): 41–47.

6. Kiefner, J. F. 1988. Effects of flowing product on line weldability. *Oil & Gas Journal* 86(29): 49–54.

7. Cola, M. J., Kiefner, J. F., Fischer, R. D., Bubenik, T. A., Jones, D. J., and Bruce, W. A. 1991. Development of simplified weld cooling rate models for in-service gas pipelines. Final Report PR-185-914. American Gas Association.

8. Goldak, J. A., Oddy, A. S., and Dorling, D. V. 1992. Finite element analysis of welding on fluid filled, pressurized pipelines. *3rd International Conference on Trends in Welding Research*. Gatlinburg, Tenn., pp. 45–50.

9. Oddy, A. S., and McDill, J. M. J. 1999. Burnthrough prediction in pipeline welding. *International Journal of Fracture* 97: 249–261.

10. Sabapathy, P. N., Wahab, M. A., and Painter, M. J. 1999. Numerical models of in-service welding of gas pipelines. *International Conference on Advances in Materials and Processing Technologies*, pp. 663–674.

11. Kim, Y.-P., Baek, J. H., and Kim, W.-S. 1999. Allowable heat input and mechanical properties of repair weld by direct deposition of weld metal. *Proc. 18th International Conference on Offshore Mechanics and Arctic Engineering*, pp. 157–164.

12. Kim, W.-S., Kim, Y.-P., and Baek, J.-H. 1999. A study on the development of repair procedure for gas pipelines. Final Report. KOGAS.

13. *ABAQUS User's Manual*. 1999. Hibbit, Karlson & Sorensen, Inc.

14. Hong, J. K., Tsai, C.-L., and Dong, P. 1998. Assessment of numerical procedures for residual stress analysis of multipass welds. *Welding Journal* 77(9): 372-s to 382-s.

15. Jonsson, M., and Josefson, B. L. 1988. Experimentally determined transient and residual stresses in a butt-welded pipe. *Journal of Strain Analysis* 108: 352–366.

16. Goldak, J., Chakravarti, A., and Bibby, M. 1984. A new finite element model for welding heat sources. *Metall. Trans. B*. 15B: 299–305.

17. Schwerdtfger, K., and Harste, K. 1988. Calculation of material data from the chemical composition. Internal report. Inst. fur Allgemeine Metallurgie, Technical University Clausthal.

18. Acadams, W. H. 1954. *Heat Transmission.* New York, N. Y.: McGraw-Hill.

19. Troive, L., and Jonsson, M. 1994. Numerical and experimental study of residual deformation due to double-J multiple-pass butt-welding of a pipe-flange joint. *Proc. IEMS '94, Annual International Conference on Industry*, pp. 107–114.

20. Bailey, N. 1970. Welding procedures for low-alloy steels. Cambridge, England: The Welding Institute, Abington Hall.

21. Graville, B. A., and Read, J. A. 1974. Optimization of fillet weld sizes. *Welding Journal* 53(4): 161-s to 169-s.

22. Felix, R. D., Bruce, W. A., and Threadgill, P. L. 1991. Development of procedures for hot tap welding onto sour service pipelines. *Proc. International Arctic Technology Conference*, pp. 349–359.

23. Tronskar, J. P. 1995. Evaluation of methods to predict safe welding conditions and maximum HAZ hardness in steel welding. *Journal of Offshore Mechanics and Arctic Engineering* 117(1): 46–56.

24. Kasuya, T., Yurioka, N., and Okumura, M. 1995. Methods for predicting maximum hardness of heat-affected zone and selecting necessary preheat temperature for steel welding. Nippon Steel Technical Report 65(4): 7–14.

25. Bang, I.-W., Oh, K. H., Kim, Y.-P., and Kim, W.-S. The effect of welding conditions on allowable heat input in bead-on-plate welding of pipeline steel. To be published.

26. Lundin, C. D., Gill, T. P. S., Qiao, C. Y. P., Wang, Y., and Khan, K. K. 1990. Weldability of low-carbon micro-alloyed steels for marine structures. *Welding Research Council Bulletin* 359: 1–103.